Inorganic Chemistry

Article

pubs.acs.org/IC

A Pyridine-Based Ligand with Two Hydrazine Functions for Lanthanide Chelation: Remarkable Kinetic Inertness for a Linear, Bishydrated Complex

Célia S. Bonnet,*[,†] Sophie Laine,[†] Frédéric Buron,[‡] Gyula Tircsó,[†,∥,⊥] Agnès Pallier,[†] Lothar Helm,[§] Franck Suzenet,[‡] and Éva Tóth*[,†]

[†]Centre de Biophysique Moléculaire, CNRS, rue Charles Sadron, 45071 Orléans, France

[‡]Université d'Orléans and CNRS, Institut de Chimie Organique et Analytique, UMR 7311 rue de Chartres, F-45067 Orléans, France

[§]Laboratory of Inorganic and Bioinorganic Chemistry, Ecole Polytechnique Fédérale de Lausanne, BCH, 1015 Lausanne, Switzerland

[∥]Department of Inorganic and Analytical Chemistry, University of Debrecen, Egyetem tér 1, 4010 Debrecen, Hungary

[⊥]Le Studium, Loire Valley Institute for Advanced Studies, 1 Rue Dupanloup, 45000 Orléans, France

Supporting Information

ABSTRACT: To study the influence of hydrazine functions in the ligand skeleton, we designed the heptadentate HYD ligand (2,2′,2″,2‴-(2,2′-(pyridine-2,6-diyl)bis(2-methylhydrazine-2,1,1-triyl)) tetraacetic acid) and compared the thermodynamic, kinetic, and relaxation properties of its Ln^{3+} complexes to those of the parent pyridine (Py) analogues without hydrazine (Py = 2,6-pyridinebis-(methanamine)-*N*,*N*,*N*′,*N*′-tetraacetic acid). The protonation constants of HYD were determined by pH-potentiometric measurements, and assigned by a combination of UV−visible and NMR spectroscopies. The protonation sequence is rather unusual and illustrates that small structural changes can strongly influence ligand basicity. The first protonation step occurs on the pyridine nitrogen in the basic region, followed by two hydrazine nitrogens and the carboxylate groups at acidic pH. Contrary to Py, HYD self-aggregates through a pH-dependent process (from pH ca. 4). Thermodynamic stability constants have been obtained by pH-potentiometry and UV−visible spectrophotometry for various Ln^{3+} and physiological cations (Zn^{2+}, Ca^{2+}, Cu^{2+}). LnHYD stability constants show the same trend as those of LnDTPA complexes along the Ln^{3+} series, with log K = 18.33 for Gd^{3+}, comparable to the Py analogue. CuHYD has a particularly high stability (log K > 19) preventing its determination from pH-potentiometric measurements. The stability constant of CuPy was also revisited and found to be underestimated in previous studies, highlighting that UV−visible spectrophotometry is often indispensable to obtain reliable stability constants for Cu^{2+} chelates. The dissociation of GdL, assessed by studying the Cu^{2+}-exchange reaction, occurs mainly via an acid-catalyzed process, with limited contribution from direct Cu^{2+} attack. The kinetic inertness of GdHYD is remarkable for a linear bishydrated chelate; the 25-fold increase in the dissociation half-life with respect to the monohydrated commercial contrast agent GdDTPA ($t_{1/2}$ = 5298 h for GdHYD vs 202 h for GdDTPA) is related to the rigidity of the HYD ligand due to the pyridine and methylated hydrazine functions of the backbone. A combined analysis of variable-temperature ^{17}O NMR and NMRD data on GdHYD yielded the microscopic parameters influencing relaxation properties. The high relaxivity (r_1 = 7.7 mM^{-1} s^{-1} at 20 MHz, 25 °C) results from the bishydrated character of the complex combined with an optimized water exchange rate (k_{ex}^{298} = 7.8 × 10^6 s^{-1}). The two inner-sphere water molecules are not replaced through interaction with biological cations such as carbonate, citrate, and phosphate as monitored by ^1H relaxivity and luminescence lifetime measurements.

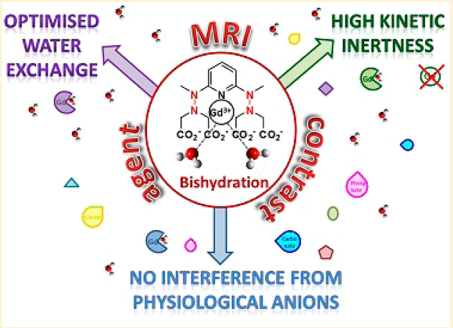

INTRODUCTION

Thanks to their unique magnetic and optical properties, the chemistry of lanthanide ions has attracted great interest over the years in the domains of medicine, telecommunication, magnetic materials, lasers, and biosciences, to cite just a few.[1] Among these, magnetic resonance imaging (MRI) uses Gd^{3+} chelates on a daily basis as contrast agents (CA). Because of its intrinsic toxicity, Gd^{3+} (and any Ln^{3+}) has to be encapsulated in thermodynamically stable and kinetically inert complexes. The structure of the ligand also affects the CA efficacy of the complex, expressed as proton relaxivity. Key parameters that influence relaxivity include the number of water molecules directly coordinated to the Gd^{3+} ion, their exchange rate with bulk water, the rotational correlation time of the complex, and its electronic relaxation. All of these parameters are related to the structural features of the complex.[2] It is therefore highly

Received: April 9, 2015
Published: June 1, 2015

DOI: 10.1021/acs.inorgchem.5b00804
Inorg. Chem. 2015, 54, 5991−6003

Chart 1. Chemical Structures of HYD and Other Ligands Discussed in This Work

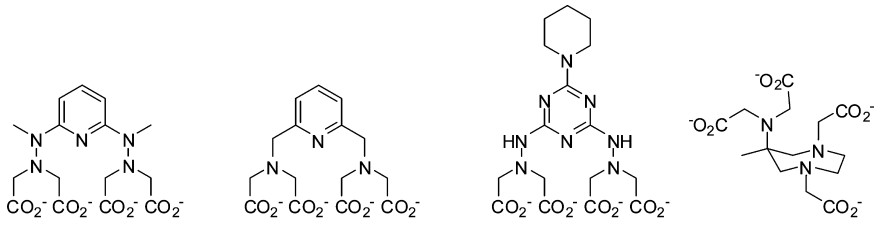

important to rationalize structure−efficacy relationships to design more efficient CA.

The need for stable complexation has prompted research for hexa-, hepta-, and octa-dentate ligands, able to match the high coordination number of Ln^{3+} ions. Classically, either acyclic (DTPA (diethylenetriaminepentaacetic acid) and its derivatives) or cyclic (DOTA (1,4,7,10-tetraazacyclododecane-1,4,7,10-tetraacetic acid) and its derivatives) poly(aminocarboxylate) ligands are used as MRI contrast agents. Both types of ligands coordinate Gd^{3+} in an octadentate manner, forming kinetically inert and thermodynamically stable complexes, with one water molecule in the first coordination sphere of Gd^{3+}. Important effort has been devoted to modify the structure of the two parent complexes, GdDOTA and GdDTPA, to improve their relaxation properties. Fundamentally different coordination modes have been also explored for Gd^{3+}, several of them allowing for more than one water molecule in the inner sphere, thus yielding higher relaxivities. An attractive idea for biocompatibility and low toxicity was to use biologically inspired ligands, such as peptides,[3,4] sugars (cyclodextrins),[5] or siderophores.[6] In the case of peptides and cyclodextrins, the hydrogen-bonding network of these highly hydrophilic complexes was beneficial for the relaxivity properties, but, unfortunately, the stability of the complexes was too low for in vivo use.[3,5,7] Ligands from the hydroxypyridinone family (HOPO) were also suggested as MRI CA.[8] Their lanthanide complexes show good thermodynamic stabilities, but their kinetic inertness is likely limited. The AAZTA (6-amino-6-methylperhydro-1,4-diazepine tetraacetic acid) family combines favorable properties both in thermodynamic stability and in kinetic inertness of the corresponding complexes that render them attractive candidates for MRI CA design.[9]

We have recently reported on pyridine-based polyaminocarboxylate ligands for Ln^{3+} complexation. They represent a versatile platform that was exploited to create bimodal contrast agents for MRI (Gd^{3+} complex) and NIR optical imaging (Nd^{3+} and Yb^{3+} complexes).[10−12] The modification of the pyridine via triazole or isoquinoline moieties allowed the optimization of the NIR luminescent properties. The derivatization of one of the pendant arms to append a Zn^{2+} complexing unit made it possible to achieve Zn^{2+} sensing through this system.[13] Despite the two water molecules in the first coordination sphere of Gd^{3+} that ensure optimized MRI properties, the complex retains good thermodynamic stability and kinetic inertness.[11] The water exchange rate is also optimized as compared to commercial contrast agents, and the two water molecules are not replaced by endogenous anions. This has prompted us to explore how further structural modifications in the skeleton affect the coordination properties. In the HYD ligand (2,2′,2″,2‴-(2,2′-(pyridine-2,6-diyl)bis(2-methylhydrazine-2,1,1-triyl)) tetraacetic acid), the amine functions of the aminopolycarboxylate pendant arms have been replaced by hydrazine, leading to drastic modification of ligand basicity (Chart 1). So far, a single example of a hydrazine-derivative ligand has been reported for Ln^{3+} complexation. It is based on a triazine bearing various substituents;[14−16] however, the influence of the hydrazine function has not been directly assessed.

In this work, we report the synthesis of ligand HYD and a detailed structural, thermodynamic, and kinetic study of its complexes formed with Ln^{3+} and endogenous cations. We have characterized the relaxation properties of the Gd^{3+} analogue in aqueous solution by ^{1}H relaxometry and ^{17}O NMR, and the effect of endogenous anions on the relaxation properties has been investigated. Comparison to the parent Py complexes allows one to conclude the influence of hydrazine on the complexation properties.

RESULTS AND DISCUSSION

1. Synthesis. The synthesis of HYD was achieved from commercially available 2,6-dibromopyrdine **1** (Scheme 1). The

Scheme 1. Synthesis of Ligand HYD

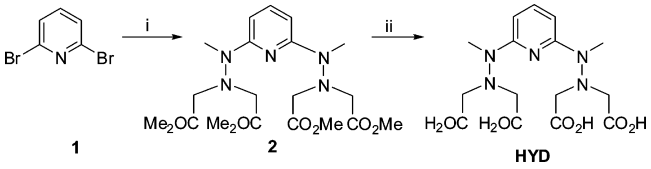

2,6-bis(1-methylhydrazinyl)pyridine was obtained by refluxing 2,6-dibromopyridine in *N*-methylhydrazine for 24 h. Because of its air and moisture sensitivity, this intermediate was directly engaged in the following alkylation step. The two hydrazine functions were reacted with methyl bromoacetate in the presence of diisopropylethylamine (DIPEA) in toluene at 75 °C for 48 h to give **2** in 42% overall yield. Saponification of methyl esters afforded ligand HYD in 90% yield after purification on ion-exchange resin. Py was synthesized following literature methods.[10,17]

2. Characterization of the Ligand. *Potentiometric Determination of the Protonation Constants.* Potentiometric titrations in KCl 0.1 M at 298 K show the presence of six protonation constants for HYD (log K_{Hi}, eq 1). The titration curve is presented in Figure 1, and the corresponding calculated values are shown in Table 1, together with those of PTDITA, Py (Chart 1), and DTPA.

$$K_{Hi} = \frac{[H_iL]}{[H_{i-1}L][H]} \quad (1)$$

DOI: 10.1021/acs.inorgchem.5b00804
Inorg. Chem. 2015, 54, 5991−6003

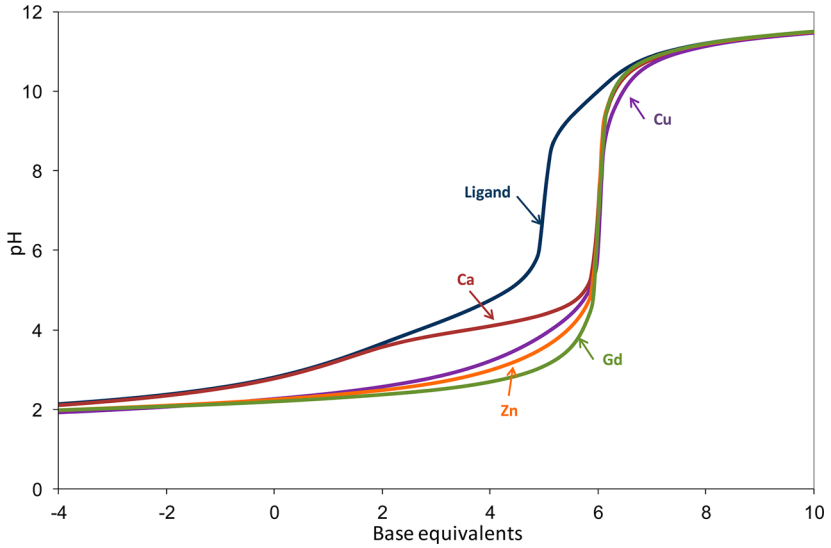

Figure 1. Potentiometric titration curves of solutions containing [HYD] = 1.79 mM with 0 or 1 equiv of $CaCl_2$, $ZnSO_4$, $CuCl_2$, or $GdCl_3$ in KCl 0.1 M at 298 K.

Table 1. Protonation Constants Measured in KCl 0.1 M at 298 K

log K_H	HYD	PTDITA[a]	Py[b]	DTPA[c]
log K_{H1}	9.30(7)	8.05	8.95	10.59
log K_{H2}	4.95(5)	4.71	7.85	8.65
log K_{H3}	4.26(8)	4.02	3.38	4.28
log K_{H4}	3.94(6)	3.36	2.48	2.73
log K_{H5}	3.29(7)	3.00		2.06
log K_{H6}	2.6(1)	1.92		
Σlog K_{Hi}	28.34	25.06	22.66	28.31

[a]From ref 15. [b]From ref 10. [c]From ref 18.

The total basicity of HYD is comparable to that of DTPA, and higher than those of PTDITA and Py. The attribution of the protonation sequence is not straightforward. For example, in the parent Py compound, the protonation constant of the nitrogen atom of the pyridine function is too low to be observed.[10] In HYD, it is expected to be totally different as the presence of nitrogen atoms in ortho position enhances the basicity of pyridine in accordance with inductive and resonance effects, and this protonation could be potentially observed. In PTDITA, the protonation order had been determined as follows: two hydrazine distal nitrogen atoms (distance to the triazine), the piperidine nitrogen atom, and carboxylate functions.[15] The protonations of the proximal, secondary nitrogens of the hydrazine functions are not observed, probably because they occur at too high pH. In contrast, in HYD these are tertiary nitrogens with expectedly lower basicity, making those protonation constants potentially observable. Consequently, we have combined pH-dependent UV−visible spectroscopy and NMR measurements to determine the protonation sequence of HYD.

UV and NMR Studies of the Ligand. The UV−visible spectrum of HYD displays several absorption bands; at neutral pH the lowest energy band is centered at 330 nm, with a sideband at 350 nm (Figure 2). It is interesting to note that the bathochrome shift as compared to the parent Py (60−70 nm) is important and similar to that observed for isoquinoline compounds, suggesting an extended π-system for this complex as compared to Py.[12]

The UV−visible spectrophotometric titration of the ligand as a function of pH shows important changes. At acidic pH, the main band is centered at 344 nm. Upon increasing pH, this band first undergoes a slight bathochromic shift and an intensity decrease, followed by an important hypsochromic shift of ca. 20 nm. The most important changes occur at pH 4−6 and 9−10 (Figure 2), corresponding respectively to the third (4.26), second (4.95), and first (9.30) protonation constants.

The absorption spectrum of the ligand is most likely affected by the protonation of the pyridine nitrogen and of the four hydrazine nitrogen atoms. The protonation of the pyridine is expected to occur at higher pH than that of 2-aminopyridine (6.86)[19] due to more important inductive and resonance effects, and can consequently be attributed to log K_{H1} = 9.30. The log K_H of 4.26 and 4.95 can then be attributed either to distal or to proximal nitrogen atoms of the hydrazine (distance to the pyridine). This is consistent with a previous observation of log K_H of distal nitrogen atoms.[15] For the proximal nitrogen, we can refer for comparison to log K_H = 7.24 of the amine function of *para*-diethylaminetoluene.[20] With respect to this molecule, in HYD, the ethyl arm is replaced by a dimethylcarboxylate amine, and the benzene by a pyridine, both with electron-withdrawing effects. This will decrease the log K_H, which is then expected to be lower than 7.24.

To determine whether the distal or proximal nitrogen atoms or both are protonated in the pH range 4−5, ^{1}H NMR titrations of the ligand were performed as a function of pH (Supporting Information Figures S3−8). Below pH ≈ 3.5, the signal of the CH_2COO appears as an AB spin pattern (3.95−3.85 ppm), indicating that the rotation of these arms is highly limited. At higher pH, this phenomenon disappears at ambient temperature, but is observed again when the temperature is decreased. This could be explained by intra- or intermolecular hydrogen bonds, restraining free rotation of the carboxylate arms. Unfortunately, at pH > 4, the H2 signal broadens with increasing pH and decreasing temperature (cf. Supporting Information Figure S11 for numbering), which is attributed to self-aggregation of the ligand. Aggregation is also evidenced by the self-diffusion coefficients of the ligand measured in D_2O at various pH (Table 2), showing an ca. 8% decrease from pH 2.24 to 6.48. As a comparison, the self-diffusion coefficient of

DOI: 10.1021/acs.inorgchem.5b00804
Inorg. Chem. 2015, 54, 5991−6003

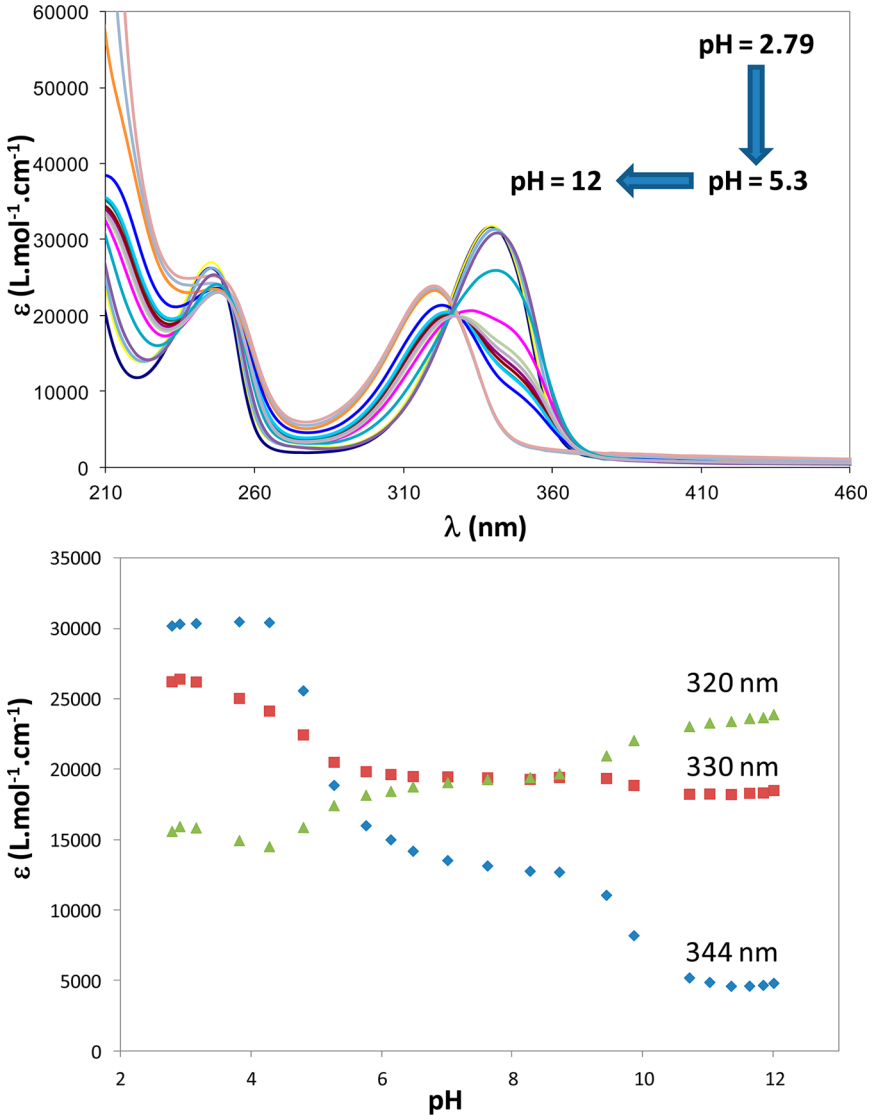

Figure 2. Absorption spectra of HYD at 11 μM, KCl 0.1 M, 298 K (pH = 2.79−12) (top), and titration curves derived at 320 nm (green ▲), 330 nm (red ■), and 344 nm (blue ◆).

Table 2. Self-Diffusion Coefficients of HYD (7 mM) Measured by NMR in D_2O at 9.4 T and 298 K

pD	2.24	5.27	6.48
$D^T/10^9$ m^2 s^{-1}	0.423(8)	0.405(9)	0.390(9)

Py was measured at neutral pH (0.424×10^{-9} m^2 s^{-1}) and was found to be comparable to that of HYD at low pH, but significantly higher than that at neutral pH (Supporting Information Table S1). UV−visible absorption spectra were also recorded as a function of concentration at various pHs, clearly evidencing aggregation at neutral pH (Supporting Information Figure S12). To rule out concentration effects, the UV−visible pH titration was performed at two different concentrations, and the trend observed in the changes of the 344 nm-absorption band is the same, confirming that they can be mainly attributed to protonation effects (Supporting Information Figure S13). Different ligand concentrations were tested for the NMR pH titration, but even at 1 mM, aggregation leads to the disappearance of the ^{1}H NMR spectrum around pD 4−5, making it impossible to attribute the protonation sequence by this technique.

To observe more directly the protonation of the nitrogen atoms, ^{1}H−^{15}N HMBC spectra were recorded on a 700 MHz NMR spectrometer equipped with a cryoprobe (Figure 3 and Supporting Information Figure S9). Between pD = 2.44 and 4.60, a clear shift to higher frequencies is observed for the proximal nitrogen of the hydrazine, whereas the signal of the distal nitrogen does not shift. This suggests that the third protonation occurs at the proximal nitrogen, which is consistent with UV observation. Although at higher pD the signals become too broad, it can be proposed that the second protonation occurs at the opposite distal nitrogen. This is supported by ^{13}C NMR spectra showing a shift between pD = 2.24 and 6.48 for NCH_2COO^- (Supporting Information Figure S10).

To sum up on the protonation sequence, the UV−visible absorption and NMR data suggest that the first protonation occurs on the pyridine, while the second and third steps occur on the distal and the opposite proximal nitrogens of the hydrazine, respectively. The last three steps might likely be attributed to the carboxylate functions as no UV changes are observed in this pH range, but both ^{13}C and ^{1}H shifts are

DOI: 10.1021/acs.inorgchem.5b00804
Inorg. Chem. 2015, 54, 5991−6003

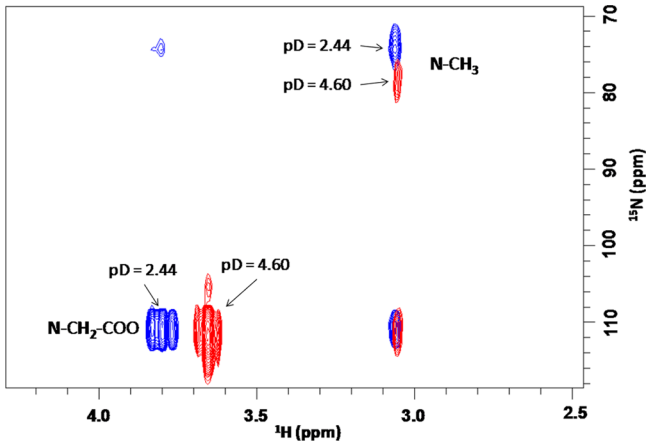

Figure 3. Comparison of partial two-dimensional $^{1}H/^{15}N$ HMBC spectra for HYD (12 mM, 700 MHz) at pD = 2.44 (blue) and pD = 4.60 (red).

observable for the CH_2COO^- arm. This protonation sequence is very different from that observed for Py, PTDITA, or classical polyaminocarboxylate ligands, illustrating that minor structural changes can drastically affect ligand basicity. Likewise, while self-aggregation is significant for HYD, it is totally absent for the parent Py.

3. Characterization of the Complexes. *Stability Constants of the Complexes.* Complex stability and protonation constants, log K_{ML} and log K_{MLH} (eqs 2 and 3), have been determined by pH-potentiometric titrations for various Ln^{3+} ions (Figure 1, Supporting Information Figures S14,15, and Table 3).

$$K_{MmL} = \frac{[M_mL]}{[M_{m-1}L][M]} \quad (2)$$

$$K_{MmLHi} = \frac{[M_mL]}{[M_mLH_{i-1}][H]} \quad (3)$$

$$K_{MLOH} = \frac{[ML]}{[ML(OH)][H]} \quad (4)$$

For all Ln^{3+} ions, nonprotonated and monoprotonated mononuclear complexes are observed. Above pH = 10, the titration curves of the lanthanide complexes all show a deprotonation step, indicating the formation of a monohydroxo complex characterized by the protonation constant K_{MLOH} (eq 4). The stability constant of the Gd^{3+} complex is comparable to that of the parent GdPy and that of GdPTDITA.[11,15] This leads to a pGd of 17.4 similar to that of the Py complex, but lower than that of PTDITA due to the higher basicity of HYD. Along the Ln^{3+} series, the stability constants increase by ca. 4 orders of magnitude until the middle of the series (Tb^{3+}), then they decrease by ca. 1 order of magnitude until the end (Figure 4). The increase of the stability constant up to Tb^{3+} can be explained by an increasing charge density of the cation as observed for flexible chelates such as EDTA. The drop of stability toward the end of the lanthanide series can be ascribed to the rigidity of HYD as compared to EDTA, implying that HYD cannot wrap efficiently around the smaller lanthanide cations. The same trend is observed for DTPA complexes.[18,21]

For all complexes, a protonation step is observed between pH 2.9 and 3.5, and might be ascribed to the protonation of a noncoordinating nitrogen atom or carboxylate function. The deprotonation at pH > 10 occurs likely on a Ln^{3+}-coordinated water molecule to yield soluble hydroxo complexes. Interestingly, the log K_{MLH} and log K_{MLOH} values are relatively constant along the Ln^{3+} series, and thus independent of the increasing acidity of the metal.

The stability constants formed with biogenic cations such as Ca^{2+}, Cu^{2+}, and Zn^{2+} have also been assessed (Figure 1, Supporting Information Figure S16, and Table 4). Indeed it has been demonstrated that in vivo toxicity of Ln^{3+} complexes is related to the release of Ln^{3+} ions, which can be a consequence of transmetalation with endogenous cations in vivo.[22] In the case of Ca^{2+}, the experimental data could well be fitted with a nonprotonated and a monoprotonated complex. For Zn^{2+}, several complex protonation constants, as well as a dinuclear complex and its protonation, had to be included in the model. The mononuclear ZnHYD complex is 1 order of magnitude more stable than the corresponding ZnPTDITA and ZnPy. The introduction of a second Zn^{2+} cation to form the bimetallic complex is more difficult due to electrostatic repulsion, which is clearly demonstrated by the considerably lower constant for this step. Similar behavior was observed for PTDITA.[15]

The case of Cu^{2+} is more complicated, as it forms very stable complexes with polyaminocarboxylate ligands. pH-potentiometric titrations have long led to underestimation of the stability, and recently it has been clearly demonstrated that UV−visible titrations (or the combination of pH-potentiometry with UV−visible spectrophotometry) are crucial to obtain

Table 3. Stability Constants Obtained with Various Ln^{3+} Ions, and pM Values Measured by Potentiometric Titrations in KCl 0.1 M at 298 K

	HYD			PTDITA[a]			Py[b]	DTPA[c]	
	log K_{ML}	log K_{MLH}	log K_{MLOH}	log K_{ML}	log K_{MLH}	log K_{MLOH}	log K_{ML}	log K_{ML}	log K_{MLH}
La^{3+}	14.91(8)	3.23(3)	10.8(1)	16.12	2.91	10.73		19.49	2.6
Ce^{3+}	16.16(8)	3.16(6)	10.9(1)					20.43	
Nd^{3+}	16.83(9)	3.27(3)	11.1(1)				18.76	21.62	2.39
Eu^{3+}	18.25(9)	3.11(2)	11.1(1)					22.39	2.15
Gd^{3+}	18.33(9)	3.06(8)	11.0(1)	18.49	2.81	10.43	18.60	22.39	2.39
Tb^{3+}	18.95(5)	2.92(7)	11.1(1)					22.72	2.14
Ho^{3+}	18.73(9)	3.05(4)	11.0(1)					22.79	2.25
Yb^{3+}	18.35(9)	3.20(8)	10.60(8)				18.39	22.64	2.3
Lu^{3+}	18.33(5)	3.46(3)	10.36(6)	17.15	2.97	9.97		22.46	2.18
pGd	17.4			18.6			17.4	19.1	

[a]From ref 15. [b]From ref 11. [c]From ref 18.

DOI: 10.1021/acs.inorgchem.5b00804
Inorg. Chem. 2015, 54, 5991−6003

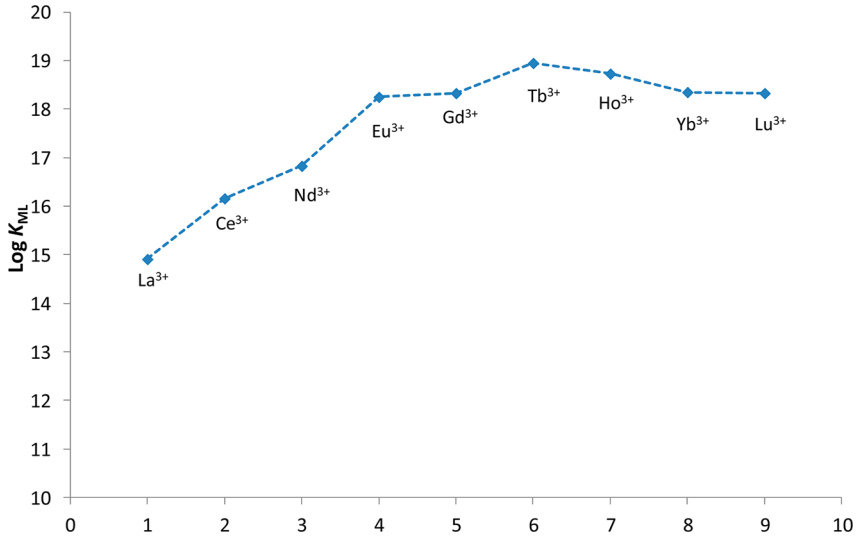

Figure 4. Thermodynamic stability constants log K_{ML} (from Table 3) of complexes formed between HYD and various lanthanide cations.

Table 4. Stability Constants Obtained with Biogenic Cations, and Selectivity Constants Measured by Potentiometric Titrations in KCl 0.1 M at 298 K

	HYD			PTDITA[a]			Py[b]			DTPA[c]		
	Ca^{2+}	Zn^{2+}	Cu^{2+}	Ca^{2+}	Zn^{2+}	Cu^{2+}	Ca^{2+}	Zn^{2+}	Cu^{2+}	Ca^{2+}	Zn^{2+}	Cu^{2+}
log K_{ML}	9.21(6)	16.27(9)	>19	9.79	15.33	15.95	9.43	15.84	17.63[d]	10.75	18.2	21.2
log K_{MLH}	3.85(9)	4.03(8)	nd[e]	3.86	3.69	3.78		3.81	3.45	6.11	5.60	4.80
log K_{MLH2}		3.0(1)	nd[e]		2.15	3.04						2.96
log K_{MLH3}			nd[e]			2.18						
log K_{MLOH}		11.08(5)	nd[e]		10.61	9.36						
log K_{M2L}		3.85(7)	nd[e]		2.75	3.48				1.6	4.48	6.79
log K_{M2LH}		3.2(1)	nd[e]			3.34						

[a]From ref 15. [b]From ref 10. [c]From ref 18. [d]Determined in NaCl 1 M. [e]Not determined.

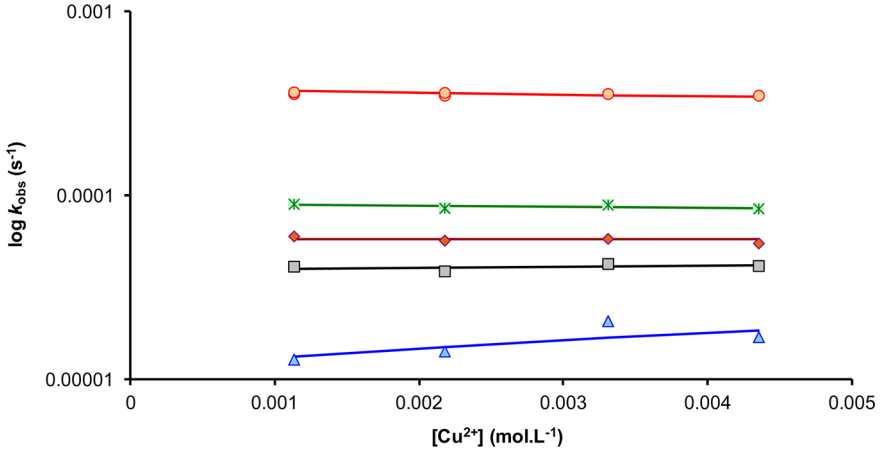

Figure 5. Log k_{obs} versus Cu^{2+} concentration for the reaction of GdHYD with Cu^{2+}. Concentration of GdHYD was 0.1 mM; pH = 3.34 (orange ●), 3.97 (green *), 4.17 (red ◆), 4.34 (gray ■), and 4.89 (blue ▲) (25 °C, 0.15 M NaCl).

reliable and unambiguous stability constants.[23,24] A major difficulty in the analysis of the pH-potentiometric data is that it is often possible to find seemingly reasonable species models that provide acceptable fitting. Typically, the presence of protonated complexes completely formed at low pH can artificially compensate for the absence of free Cu^{2+} in the sample. In the case of HYD, UV−visible measurements have been complicated by the strong absorption of the ligand in the visible range; nevertheless, we could obtain an estimation of the log K_{CuL} greater than 19.

With this new light, we have reinvestigated the stability constant of the CuPy complex. Again, the pH-potentiometric data could be fitted with a reasonable model including CuL and CuLH species (the same species found previously); however, UV−visible measurements evidenced full complex formation already below pH = 2 with an important proportion of the protonated complex. The simultaneous analysis of pH-

DOI: 10.1021/acs.inorgchem.5b00804
Inorg. Chem. 2015, 54, 5991−6003

potentiometric and UV−visible data yielded log K_{CuL} = 17.63(3), a much higher value than previously reported[10] (see Supporting Information Tables S2−S4 and Figure S17 for complete results), and the formation of a dinuclear Cu^{2+} complex was also evidenced. While the stability constant of CuPy is only slightly lower than that of CuHYD, surprisingly, a 4 orders of magnitude lower value was reported for CuPTDITA.[15]

Kinetic Inertness. Kinetic inertness is the key parameter for the in vivo safety of a Gd^{3+} complex as both dissociation products, that is, the released metal ion and the free ligand, are highly toxic. It has been emphasized in several reports that the kinetic inertness is more important than the absolute value of the thermodynamic stability constant.[25] To characterize the kinetic inertness of GdHYD, the rate of the metal exchange reaction was studied with the use of Cu^{2+} as exchanging ion. Cu^{2+} is known to most efficiently catalyze dissociation reactions among biogenic cations as it also forms stable complexes of similar or greater stability than those of Gd^{3+} complexes with most of the ligands applied in vivo.[26] The dissociation (eq 5) was monitored at pH 3.35−4.89 by using conventional UV−visible spectrophotometry in the presence of high (10−40-fold) excess of Cu^{2+} to ensure pseudo-first-order conditions.

$$[GdHYD]^{-} + Cu^{2+} \rightleftharpoons [CuHYD]^{2-} + Gd^{3+} \quad (5)$$

In the excess of the exchanging metal ion, the reaction rate can be expressed by eq 6, where k_{obs} is a pseudo-first-order rate constant and $[GdL]_t$ is the total complex concentration:

$$-\frac{d[Gd(L)]_t}{dt} = k_{obs}[Gd(L)]_t \quad (6)$$

The k_{obs} values increase with increasing concentration of H^+, but remain relatively constant (particularly at low pH) upon increasing Cu^{2+} concentration (Figure 5, and Supporting Information Figure S18). Only at the highest pH (4.89), where the acid-catalyzed dissociation of the complexes becomes less pronounced, do we observe a slight dependence of the k_{obs} on the Cu^{2+} concentration (k_{obs} can be fitted with a straight line with a positive slope). This indicates that, at this higher pH, the exchange reaction may also take place by direct attack of the exchanging metal ion on the complex via the formation of a dinuclear intermediate. All together, these experimental observations could be rationalized by considering spontaneous as well as proton- and metal-assisted dissociation for GdHYD. The overall map of dissociation is illustrated in Scheme 2.

The concentration of GdHYD can be given as the sum of the concentrations of the different reactive species (eq 7):

Scheme 2. Reaction Mechanism of the Dissociation of Gd^{3+} Complexes of DTPA-like Ligands[a]

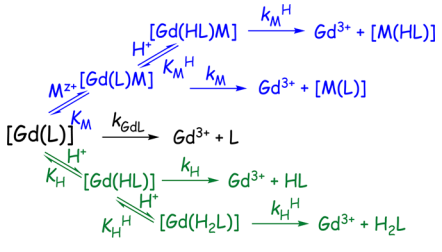

[a]Charges of the complexes are omitted for clarity.

$$[Gd(L)]_t = [GdL] + [Gd(HL)] + [Gd(H_2L)] + [Gd(L)Cu] \quad (7)$$

and hence

$$k_{obs}[Gd(L)]_t = k_{GdL}[GdL] + k_H[Gd(L)H] + k_H^H[Gd(L)H_2] + k_M[Gd(L)Cu]$$

Considering the complex protonation constants (K_H = $[GdLH]/[GdL][H^+]$ and K^H_H = $[GdLH_2]/[GdLH][H^+]$) as well as the stability constant of the dinuclear intermediate (K_M = $[GdLCu]/[GdL][Cu]$), the pseudo-first-order rate constant (k_{obs}) can be expressed as follows (eq 8):

$$k_{obs} = \frac{k_0 + k_1[H^+] + k_2[H^+]^2 + k_3[Cu^{2+}]}{1 + K_H[H^+] + K_HK_H^H[H^+]^2 + K_{Cu}[Cu^{2+}]} \quad (8)$$

where $k_0 = k_{GdL}$, $k_1 = k_HK_H$, $k_2 = k_H^HK_HK_H^H$, and $k_3 = k_{Cu}K_{Cu}$.

The dissociation scheme is very similar to that observed for GdDTPA and other Gd^{3+} complexes formed with DTPA-type ligands or with AAZTA. Figure 5 shows the best fit of the k_{obs} values to eq 8. In the fitting, the rate constant characteristic for the spontaneous dissociation (k_0) was found to be smaller than its standard deviation ($9.5 \times 10^{-9} \pm 1.4 \times 10^{-6}$ s^{-1}) and was consequently fixed to 0 in final data treatment. We were not able to determine the second protonation constant of the complex, which must be very small. Indeed, the first protonation equilibrium can be characterized by the constant of 1148 as determined by pH-potentiometric titrations, and the second protonation constant has to be even smaller (it could not be determined from pH potentiometric titration). In the pH range applied here, $K_HK^H_H[H^+]$ is likely smaller than 1 in the denominator even if we consider that $K_H = K^H_H$, and thus can be neglected. Consequently, eq 8 could be simplified, and eq 9 was used for the final data processing.

$$k_{obs} = \frac{k_1[H^+] + k_2[H^+]^2 + k_3[Cu^{2+}]}{1 + K_H[H^+] + K_{Cu}[Cu^{2+}]} \quad (9)$$

The rate constants obtained are compared to the corresponding values of GdDTPA and GdAAZTA in Table 5.

Table 5. Rate and Equilibrium Constants Characterizing the Dissociation of the Gd^{3+} Complexes of HYD, DTPA, and AAZTA (25 °C)

	HYD	DTPA[a]	AAZTA[b]
k_1 (M^{-1} s^{-1})	0.85 ± 0.03	0.58	1.05
k_2 (M^{-2} s^{-1})	908 ± 98	9.7×10^4	
k_3^{Cu} (M^{-1} s^{-1})	(2.4 ± 0.3) × 10^{-3}	0.93	1.9×10^{-4}
$K^H_{[Gd(HL)]}$	1148[c]	100[c]	233
$K^*_{[Gd(L)Cu]}$	44 ± 15	13	9
$t_{1/2}$ (h)[d]	5298	202	4585

[a]From ref 27. [b]From ref 25. [c]Determined by pH-potentiometric titration. [d]The half-lives of the Gd^{3+} complexes were calculated at physiological conditions (pH = 7.4, $c_{Cu^{2+}}$ = 1 μM).

The rate constant k_1, characterizing the proton-assisted dissociation of the complex, falls between the values measured for GdDTPA and GdAAZTA. The rate constant characterizing the pathway involving the Cu^{2+} ion, k_3, is nearly 400 times smaller for GdHYD than for GdDTPA. Surprisingly, the stability of the dinuclear intermediate is 3−4 times greater for HYD than for the corresponding DTPA and AAZTA

DOI: 10.1021/acs.inorgchem.5b00804
Inorg. Chem. 2015, 54, 5991−6003

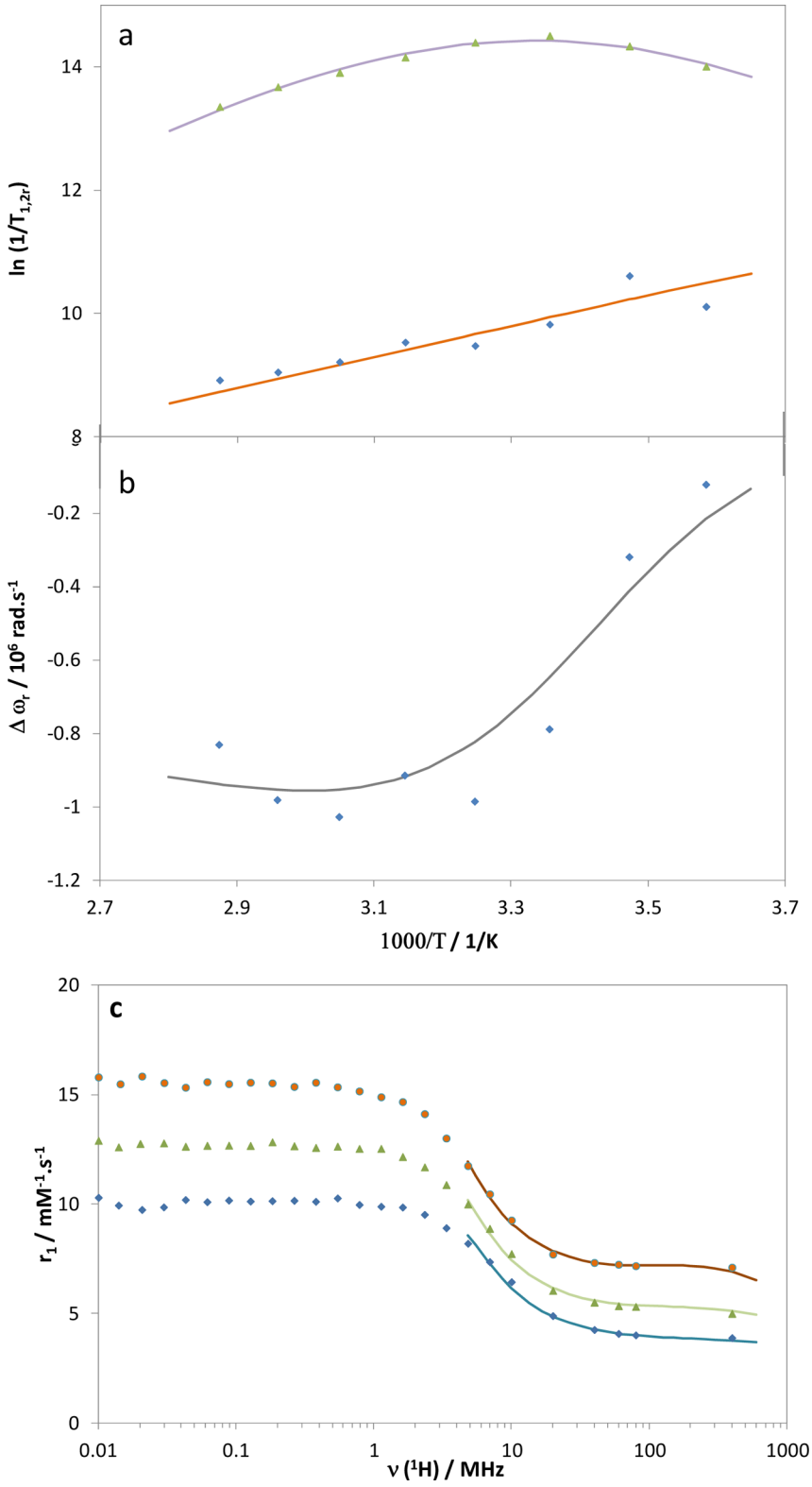

Figure 6. Temperature dependence of the reduced ^{17}O (a) transverse (green ▲) and longitudinal (blue ◆) relaxation rates, (b) chemical shifts of GdHYD at 11.7 T, and (c) NMRD profiles of GdHYD at 25 °C (orange ●), 37 °C (green ▲), and 50 °C (blue ◆). The curves represent the simultaneous fit to the experimental data points.

intermediates, but falls in the same range as those observed for some polyaminocarboxylate ligands where the two iminodiacetate arms lie closer than in DTPA.[28] This higher stability could be attributed partially to the rigidity of the ligand, which presumably results in a more preorganized coordination environment around the Gd^{3+} ion rendering the two iminodiacetate groups more independent (which in turn increases the propensity of the ligand to form dinuclear kinetic intermediates). The transmetalation of GdHYD predominantly occurs through proton-assisted dissociation of the complex with

DOI: 10.1021/acs.inorgchem.5b00804
Inorg. Chem. 2015, 54, 5991−6003

small contribution from direct attack of the exchanging metal ion. The comparison of the dissociation half-lives, $t_{1/2}$, near physiological conditions (pH = 7.4, c_{Cu}^{2+} = 1 μM; Table 5) shows remarkable kinetic inertness for GdHYD. With respect to GdDTPA, this high kinetic inertness is related to the fact that both the copper-assisted dissociation and the dissociation of the protonated complex are 2 orders of magnitude slower. It is likely the result of the rigidity of HYD, which prevents easy structural rearrangements required for the dissociation. This rigidity arises not only from the presence of the pyridine in the backbone, as was already evidenced for LnPy,[10] but also from the methyl substituents on the hydrazine.

Structure of the Complexes. To assess the structure of the Ln^{3+} complexes, we studied the diamagnetic LuHYD by NMR (see Supporting Information Figure S19) at pD = 7.16. The ^{1}H NMR spectrum shows five sets of signals pointing to C_1 symmetry of the complex. It also indicates a single major species in solution and excludes aggregation in these conditions. The complete assignments of the proton and carbon signals (see Supporting Information Figure S11 and Table S5) were based upon 2D heteronuclear HSQC and HMBC experiments. The signal of the acetate CH_2 protons (H5, see Supporting Information Figure S19) shows AB spin pattern, which confirms coordination of these arms to Lu^{3+}. The coupling constant, 16 Hz, is characteristic for the coupling of protons.

The self-diffusion coefficient of the complex at pD = 7.16 is 0.396 (5) × 10^{-9} m^2 s^{-1} in D_2O, which confirms the absence of self-aggregation. It is higher than that of the ligand alone at pD = 6.71, and slightly lower than that found for HYD in acidic conditions, as expected for a Ln^{3+} complex slightly heavier than the ligand alone. It means that the pH-dependent self-aggregation process observed for the ligand alone is prevented maybe by electrostatic repulsion between the negatively charged Ln^{3+} complexes.

To determine the hydration number of the Ln^{3+} in LnHYD, we also measured luminescence lifetimes of the corresponding Eu^{3+} complex in H_2O and D_2O. The lifetimes obtained are 0.315(4) and 0.759(5) ms in H_2O and D_2O, respectively, giving a number of water molecules directly coordinated to Eu^{3+} of 1.9,[29] very close to 2 (vide infra, Table 7). This confirms the heptadenticity of HYD.

4. Relaxometric Properties of the Gd Complex. To characterize the parameters governing proton relaxivity of the complex, nuclear magnetic relaxation dispersion (NMRD) profiles were recorded in the field range 10 kHz−400 MHz, at three different temperatures. Because the relaxivity is determined by several physicochemical parameters, including water exchange rate, electron relaxation parameters, and rotational correlation times, it is important to assess the maximum of these parameters independently. To this end, NMRD measurements are usually combined with ^{17}O NMR spectroscopy.

Variable-temperature ^{17}O T_2 measurements give access to the water exchange rate, k_{ex}. The ^{17}O T_1 data are determined by dipole−dipole and quadrupolar relaxation mechanisms and provide information about the rotational correlation time, τ_R. The ^{17}O chemical shifts give indication of the number of water molecules directly coordinated to Gd^{3+}, q.[2] Longitudinal, transverse ^{17}O relaxation rates and chemical shifts were measured as a function of the temperature on aqueous solution of GdHYD, and on a diamagnetic reference ($HClO_4$, pH 3.3) at 11.7 T. The reduced ^{17}O transverse and longitudinal relaxation rates and chemical shifts are presented in Figure 6.

The experimental ^{17}O chemical shifts evidence bishydration of the complex, which is consistent with the luminescence lifetime measurements. This is also in accordance with the relaxivity value, r_1 = 7.71 mM^{-1} s^{-1} (20 MHz, 298 K), and with the bishydrated character of the parent GdPy or GdPTDITA.[11,15] The reduced ^{17}O transverse relaxation rates first increase (up to ca. 298 K), then decrease with increasing temperature, indicating that the complex is in the slow kinetic region at low temperatures and in the fast exchange region at higher temperatures. In the slow kinetic region, $1/T_{2r}$ is directly determined by the exchange rate constant k_{ex}, whereas in the fast exchange region, it is determined by the transverse relaxation rate of the coordinated water oxygen, $1/T_{2m}$, which is in turn influenced by the water exchange rate, k_{ex}, the longitudinal electronic relaxation rate, $1/T_{1e}$, and the scalar coupling constant, $A/\hbar$. In our case, the slow kinetic region is well-defined and enables a reliable determination of k_{ex}.

The transverse and longitudinal ^{17}O relaxation rates, the ^{17}O chemical shifts, and the NMRD profiles were simultaneously analyzed with the Solomon−Bloembergen and Morgan (SBM) theory to yield the microscopic parameters characterizing water exchange and rotation (see the Supporting Information for equations). If we are not interested in detailed information about electron spin relaxation, the SBM approach can be applied to the analysis of the NMRD data at medium and high magnetic fields, and gives reliable information on dynamic processes like water exchange and rotational correlation times for small complexes.[30] Therefore, we decided to include only relaxivity values above 6 MHz in the fitting. The number of water molecules directly coordinated to Gd^{3+}, q, was fixed to 2, and several parameters have been fixed to common values. Among these, r_{GdO} has been fixed to 2.5 Å, based on available crystal structures and ENDOR results,[31] and the quadrupolar coupling constant, $\chi(1 + \eta^2/3)^{1/2}$, has been set to the value for pure water, 7.58 MHz.[32] The diffusion coefficient D^t was measured by NMR in D_2O on the corresponding Lu^{3+} complex, and the value in H_2O was scaled with the viscosity ratio $\eta(D_2O)/\eta(H_2O)$ = 1.23 according to the Stokes−Einstein formula. The diffusion coefficient $D_{GdH}^{298} = D^t + D_{H2O}$ was fixed to 2.78 × 10^{-9} m^2 s^{-1}, and the corresponding activation energy E_{DGdH} was fitted. The Gd−water proton distance was fixed to r_{GdH} = 3.1 Å, and the closest approach between the Gd^{3+} ion and the outer sphere protons to a_{GdH} = 3.6 Å. The following parameters have been adjusted: the water exchange rate, k_{ex}^{298}, the activation enthalpy for water exchange, $\Delta H^{\ddagger}$, the scalar coupling constant, $A/\hbar$, the rotational correlation time, τ_R^{298}, and its activation energy, E_R, and the parameters describing electron spin relaxation, the mean square of the zero field splitting, Δ^2, the correlation time for the modulation of the zero field splitting, τ_V^{298}, while its activation energy, E_V, has been fixed to 1 kJ/mol. The parameters resulting from the best fit are presented in Table 6 and Supporting Information Figure S6.

The fit yielded a value of k_{ex} of 7.8 × 10^6 s^{-1}, which is more than 2 times higher than that of GdPTDITA, and on the same order of magnitude than that of GdPy. The water exchange rate is optimized as compared to commercial CA such as GdDTPA or GdDOTA.[2] The relaxivity profiles as a function of temperature show a decrease of relaxivity with increasing temperature (Figure 6), which means that the relaxivity is limited by fast rotation. The fitted value of τ_R (92.6 ps) lies

DOI: 10.1021/acs.inorgchem.5b00804
Inorg. Chem. 2015, 54, 5991−6003

Table 6. Parameters Obtained from the Simultaneous Fitting of the Longitudinal, Transverse ^{17}O Relaxation Rates and Chemical Shifts as a Function of Temperature at 11.7 T, and of the NMRD Profiles at 298, 310, and 323 K

	GdHYD	GdPTDITA[a]	GdPy[b]	GdDTPA[c]
k_{ex}^{298} (10^6 s^{-1})	7.8(2)	3.3	9.3	3.3
$\Delta H^{\ddagger}$ (kJ mol^{-1})	43.5(5)	37.7	50.4	51.6
$\Delta S^{\ddagger}$ (J mol^{-1} K^{-1})	33(1)	6.4	58	53.0
τ_{RH}^{298} (ps)	92.6(9)	105	92[d]	58
E_R (kJ mol^{-1})	21.0(8)	18	20.2	17.3
q	2	2	2	1
$A/\hbar$ (10^6 rad s^{-1})	−4.0(1)	−3.3	−3.7	−3.8

[a]From ref 15. [b]From ref 11. [c]From ref 33. [d]τ_{RO}^{298}.

between that of GdPy and GdPTDITA, which correlates well with the respective sizes of the complexes.

Finally, the pH-dependence of the relaxivity was checked, and the relaxivity was found to be constant in the pH range 4–9. At pH > 9, the relaxivity decreases slightly, supporting the formation of a hydroxo-complex, likely through the deprotonation of a water molecule, as observed from pH-potentiometry.

5. Anion Interaction. For bishydrated complexes, the lack of ternary complexes, that is, the nondisplacement of water molecules by endogenous anions such as phosphate, carbonate, and citrate, is a crucial point for retaining high relaxivity in highly competitive biological media. Indeed, if one or both of the water molecules are replaced by an anion, the relaxivity will dramatically decrease.

We have monitored the relaxivity of GdHYD at pH = 7.4 (Hepes buffer), and 298 K, as a function of increasing concentration (up to 50 equiv; ca. 50 mM) of carbonate, phosphate, or citrate (Figure 7). This is well above the physiological concentration of those ions in human plasma, which are ca. 25, 1.1, and 0.11 mM for carbonate, phosphate, and citrate, respectively.

The addition of 5 equiv of phosphate resulted in a 13% decrease of the relaxivity, without significant further variation. This anion has been proved to interact in a monodentate manner (such as fluoride or acetate), and displace one coordinated water molecule.[34] To see if this small relaxivity change is due to the partial displacement of a water molecule, Eu^{3+} luminescence lifetimes were measured in the absence and in the presence of 10 equiv of phosphate (Table 7). The calculated number of water molecules is close to 2, independent of the presence of phosphate. Thus, the small relaxivity change observed could be rather attributed to the perturbation of the second sphere relaxation effect by the presence of phosphate ions via formation of hydrogen bonds to the ligand that reduces the number of second sphere water molecules or increases their distance to Gd^{3+}.

Table 7. Eu^{3+} Luminescence Lifetimes (τ) in the EuHYD Complex (0.9 mM in 0.1 M Hepes Buffer pH/pD = 7) in the Absence and in the Presence of 10 equiv of Phosphate or Carbonate, and the Corresponding Calculated q-Values

	EuHYD	EuHYD + phosphate	EuHYD + carbonate
τ_{H2O} (ms)	0.315(4)	0.324(3)	0.323(3)
τ_{D2O} (ms)	0.759(5)	0.797(5)	0.69(1)
q^a	1.9(5)	1.9(5)	1.7(5)

[a]Obtained from the empirical formula: $q = 1.2(1/\tau_{H2O} - 1/\tau_{D2O} - 0.25)$.[29]

In contrast, carbonate and citrate typically interact with bishydrated complexes in a bidentate manner, leading to a dramatic decrease of relaxivity.[34] For GdHYD, the relaxivity remains constant upon addition of 50 equiv of carbonate or 40 equiv of citrate. This excludes the formation of ternary complexes with these anions, which was also confirmed by luminescence lifetime measurements on EuHYD in the presence of 10 equiv of carbonate (Table 7).

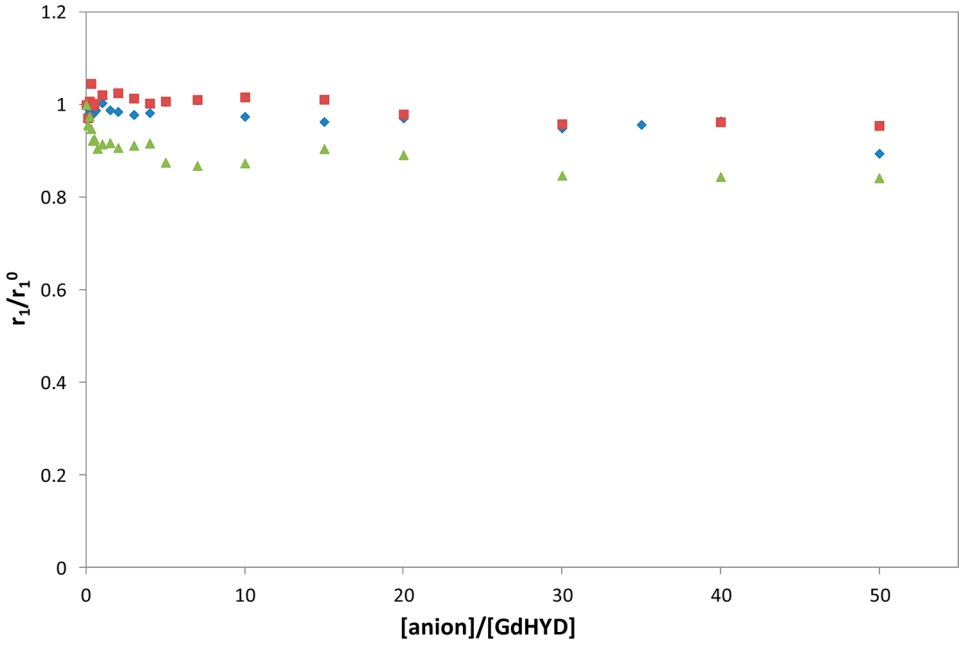

Figure 7. Relaxivities measured (298 K, pH = 7.4 in Hepes buffer 0.1 M) in the presence of GdHYD (1.28 mM) and normalized to the initial value as a function of the concentration of citrate (blue ◆, 20 MHz), carbonate (red ■, 6 MHz), and phosphate (green ▲, 6 MHz).

DOI: 10.1021/acs.inorgchem.5b00804
Inorg. Chem. 2015, 54, 5991–6003

The absence of ternary complex formation with physiological anions could be explained by electrostatic repulsion between the negatively charged Gd^{3+} complex and the anions, as previously observed.[16,35] Nevertheless, weak interactions had been observed between the negatively charged GdPTDITA and citrate (34% relaxivity decrease) or carbonate.[15] Consequently, the electrostatic repulsion is not the only factor; the relative position of the two water molecules in GdHYD is certainly not adapted for anion binding, especially for bidentate interactions. The absence of ternary complexes had been previously observed for the parent GdPy complex as well.[10]

Taken together, these data suggest that small changes in the coordination sphere of the Gd^{3+} (the coordination spheres of PTDITA and HYD are very similar) can lead to important differences in the properties of the complexes toward anion binding.

CONCLUSION

We have synthesized and characterized a pyridine-based compound containing two methylhydrazinodiacetate moieties for Gd^{3+} complexation. The introduction of the hydrazine functions leads to pH-dependent self-aggregation of the ligand, evidenced by means of UV−visible and ^{1}H NMR spectroscopies. The protonation constants of the ligand were determined by pH-potentiometry and assigned by UV−visible spectroscopy combined with ^{1}H, ^{13}C, and ^{15}N NMR. The protonation sequence is rather unusual and involves the sequential protonation of the pyridine, a distal nitrogen and an opposite proximal nitrogen of the hydrazine, followed by the carboxylates. The thermodynamic stability of the complexes was assessed by pH-potentiometry, combined with UV−visible measurements in the case of Cu^{2+}. The stability constant of the CuPy complex, largely underestimated in previous reports, was also revisited. The importance of systematic UV−visible titrations in very acidic pH range is evidenced for the determination of Cu^{2+} stability constants. The similar stability constants obtained for GdHYD and GdPy prove a limited influence of the hydrazine functions on the stability of the Ln^{3+} complexes. The kinetic inertness of GdHYD, assessed by relaxivity measurements in Cu^{2+} exchange reactions, is remarkably high, with a 25-fold increase in the dissociation half-life as compared to the commercial contrast agent GdDTPA.

NMR data on the diamagnetic LuHYD show a single major species in solution and exclude aggregation. Variable-temperature ^{17}O NMR, luminescence lifetime, and proton relaxivity data proved the bishydrated character of the Gd^{3+} complex endowed with a high water exchange rate. Physiological anions such as phosphate, citrate, or carbonate practically do not affect the number of inner sphere water molecules, as evidenced by luminescence lifetime measurements on EuHYD, and consequently have no significant effect on the relaxivity of the Gd^{3+} analogue.

Although low thermodynamic stability would prevent in vivo use of GdHYD, its kinetic inertness is truly remarkable, and physiological anions do not alter its relaxation efficacy. Most importantly, this study demonstrates how small changes in simple ligand structures can significantly modify the physicochemical properties of ligands and their corresponding complexes.

EXPERIMENTAL SECTION

Synthesis. All reagents were purchased from commercial suppliers and were used without further purification. ^{1}H NMR and ^{13}C NMR spectra were recorded on a Bruker DPX 400 MHz instrument using $CDCl_3$ or DMSO-d_6. The chemical shifts are reported in parts per million (δ scale), and all coupling constant (J) values are in Hertz (Hz). The following abbreviations were used to explain the multiplicities: s (singlet), d (doublet), t (triplet), q (quartet), m (multiplet), and dd (doublet doublet). Melting points are uncorrected. IR absorption spectra were obtained on a PerkinElmer PARAGON 1000 PC, and values are reported in cm^{-1}. HRMS was recorded on a Bruker maXis mass spectrometer. Monitoring of the reactions was performed using silica gel TLC plates (silica Merck 60 F254). Spots were visualized by UV light at 254 and 356 nm. Column chromatographies were performed using silica gel 60 (0.063−0.200 mm, Merck).

Tetramethyl 2,2′,2″,2‴-(2,2′-(Pyridine-2,6-diyl)bis(2-methylhydrazine-2,1,1-triyl))tetraacetate ***2***. 5 mL of methylhydrazine was added to 2,6-dibromopyridine **1** (2.0 g, 8.5 mmol) under N_2. The reaction mixture was stirred for 24 h at 80 °C and then evaporated to give 1 g (71%) of 2,6-bis(1-methylhydrazinyl)pyridine as a white solid. This product is not air and moisture stable. Methylbromoacetate (1.4 mL, 8.0 equiv) was added to a vigorously stirred solution of 2,6-bis(1-methylhydrazinyl)pyridine (0.31 g, 1.9 mmol) and DIPEA (1.3 mL, 4.0 equiv) in toluene (60 mL) under N_2. The reaction mixture was stirred for 48 h at 75 °C. The residue was cooled and filtered. The filtrate was evaporated, and the residue was purified by flash chromatography on silica gel (CH_2Cl_2/AcOEt 95:5 and finished with AcOEt) to give 0.5 g (59%) of tetramethyl 2,2′,2″,2‴-(2,2′-(pyridine-2,6-diyl)bis(2-methylhydrazine-2,1,1-triyl))tetraacetate as a yellow liquid (overall yield 42%). ^{1}H NMR (400 MHz, $CDCl_3$): δ 7.33 (t, J = 8.0 Hz, 1H), 6.65 (d, J = 8.0 Hz, 2H), 3.74 (s, 8H, 4×CH_2), 3.62 (s, 12H, 4×CH_3), 3.01 (s, 6H, 2×NCH_3). ^{13}C NMR (101 MHz, $CDCl_3$): δ 170.8 (Cq), 158.5 (Cq), 138.9 (CH), 98.2 (CH), 54.4 (CH_2), 51.7 (CH_3), 30.4 (CH_3). IR (ATR diamond, cm^{-1}) ν: 2957, 2849, 1729, 1577, 1476, 1431, 1200, 1019, 993, 797, 730. HRMS (EI−MS) m/z calcd for $C_{19}H_{30}N_5O_8$ $[M + H]^+$, 456.2015; found, 456.2027.

2,2′,2″,2‴-(2,2′-(Pyridine-2,6-diyl)bis(2-methylhydrazine-2,1,1-triyl))tetraacetic Acid (HYD). LiOH (0.76 g, 12 equiv) was added to a solution of tetramethyl 2,2′,2″,2‴-(2,2′-(pyridine-2,6-diyl)bis(2-methylhydrazine-2,1,1-triyl))tetraacetate **2** (1.2 g, 2.63 mmol) in a mixture THF/H_2O (1:1, 20 mL). The mixture was stirred at room temperature during 16 h. The organic solvent was evaporated, and the aqueous mixture was purified on an anionic exchange resin (DOWEX 1X2-100Cl) (washed with H_2O/MeOH 90/10, and eluted with formic acid) to obtain 2,2′,2″,2‴-(2,2′-(pyridine-2,6-diyl)bis(2-methylhydrazine-2,1,1-triyl))tetraacetic acid HYD as a red solid (0.94 g, 90%). Mp: degradation. ^{1}H NMR (400 MHz, DMSO-d_6): δ 7.35 (t, J = 8.1 Hz, 1H), 6.60 (d, J = 8.1 Hz, 2H), 3.60 (d, J = 5.7 Hz, 8H, 4×CH_2), 2.97 (s, 6H, 2×NCH_3). ^{13}C NMR (101 MHz, DMSO-d_6): δ 171.6 (Cq), 157.8 (Cq), 139.0 (CH), 97.6 (CH), 54.6 (CH_2), 29.1 (CH_3). IR (ATR diamond, cm^{-1}) ν: 2897, 2525, 1753, 1616, 1390, 1303, 1214, 810, 724. HRMS (EI−MS) m/z calcd for $C_{15}H_{22}N_5O_8$ $[M + H]^+$, 400.1468; found, 400.1481.

Liquid Sample Preparation. The ligand concentrations were determined by adding an excess of lanthanide solution to the ligand solution and titrating the metal excess with standardized Na_2H_2EDTA in urotropine buffer (pH 5.6−5.8) in the presence of Xylenol Orange as an indicator. The concentrations of the metal solutions were determined similarly by complexometric titrations. The concentrations of Gd^{3+}-containing solutions were also checked by both ICP-MS and BMS measurements when possible.

Potentiometric Studies. Carbonate-free 0.1 mol L^{-1} KOH and 0.1 mol L^{-1} HCl were prepared from Fisher Chemicals concentrates. Potentiometric titrations were performed in 0.1 mol L^{-1} aqueous KCl under nitrogen atmosphere, and the temperature was controlled to 25 ± 0.1 °C with a circulating water bath. The p[H] (p[H] = −log[H^+], concentration in molarity) was measured in each titration with a combined micro pH glass electrode (Metrohm 6.0224.100) filled with 3 M KCl, and the titrant addition was automated by use of a 702 SM

DOI: 10.1021/acs.inorgchem.5b00804
Inorg. Chem. 2015, 54, 5991−6003

titrino system (Metrohm). The electrode was calibrated in hydrogen ion concentration by titration of HCl with KOH in 0.1 mol L^{-1} electrolyte solution.[36] A plot of meter reading versus p[H] allows the determination of the electrode standard potential ($E°$) and the slope factor (f). Continuous potentiometric titrations with HCl and KOH 0.1 mol L^{-1} were conducted on aqueous solutions containing 5 mL of HYD 1.2−1.8 mM in KCl 0.1 mol L^{-1}, with 2 min waiting between successive points. The titrations of the metal complexes were performed with the same ligand solutions containing 1 or 2 equiv of metal cation, with 2 min waiting time between two points. Experimental data were refined using the computer program Hyperquad 2008.[37] All equilibrium constants are concentration quotients rather than activities and are defined as

$$K_{mlh} = \frac{[M_m L_l H_h]}{[M]^m [L]^l [H]^h}$$

The ionic product of water at 25 °C and 0.1 mol L^{-1} ionic strength is pK_w = 13.77.[18] Fixed values were used for pK_w, ligand acidity constants, and total concentrations of metal, ligand, and acid. All values and errors (one standard deviation) reported are at least the average of three independent experiments.

UV−Visible Spectroscopy. UV−visible absorption spectra were recorded on a PerkinElmer Lambda 19 spectrometer in the region λ = 200−500 nm with data steps of 1 nm, with a 1 cm path length. Measurements were performed in H_2O, KCl 0.1 M at 298 K. pH titrations were performed at 11 and 41 μM of HYD. The spectra as a function of concentration at different pH values were obtained from a stock solution of HYD of 50.85 μM in 50 mM citrate buffer (pH = 3.49), or in 50 mM acetate buffer (pH = 4.70), or in 50 mM Hepes buffer (pH = 7.11), and then diluted in the same media.

For the stability constant of the CuPy complex, out-of-cell (batch) samples were prepared containing the ligand (2.67 mM) and Cu^{2+} (2.63 mM) by applying slight ligand excess. The acidity of the samples was varied in the concentration range of 13.62−985.2 mM, and the samples were equilibrated for 3 days. The measurements were performed at 25 °C, using thermostated semimicro 1.0 cm cells. The molar absorbances of $CuCl_2$ and CuPy were determined at 21 wavelengths (570−770 nm range) by recording the spectra of 2.5 × 10^{-3}, 5.0 × 10^{-3}, 7.5 × 10^{-3}, and 1.0 × 10^{-2} M (for Cu^{2+}), and 1.32 × 10^{-3}, 2.64 × 10^{-3}, and 3.97 × 10^{-3} M (for CuPy) solutions, while the molar absorption coefficients of the protonated (CuHPy and CuH_2Py) species were calculated during the simultaneous (UV−visible and pH-potentiometric titration curves obtained at various metal to ligand concentrations) data refinement.

Lifetime Measurements. Europium luminescence lifetimes were recorded on an Agilent Cary Eclipse fluorescence spectrophotometer by recording the decay of the emission intensity at 616 nm, following an excitation at 272 nm. Measurements were performed in H_2O and D_2O solutions, for a concentration of EuHYD of 0.9 mM in Hepes buffers 0.1 M at pH/pD 7. Ten equivalents of citrate or phosphate was added to both solutions. The settings were as follow: gate time, 0.1 ms; delay time, 0.1 ms; flash count, 1; total decay time, 10 ms; 100 cycles; PMT detector, 800 mV. At least three decay curves were collected for each sample, all lifetimes were analyzed as monoexponential decays, and it was also checked that direct excitation of the metal at 396 nm gave similar results. The reported lifetimes are an average of at least three measurements.

NMR Spectroscopy. The NMR spectra were recorded on a Bruker Avance III HD 600 equipped with a BBFO probe 5 mm, and on a Bruker Avance III HD 700 equipped with a CPTCI cryoprobe 5 mm. The spectra were recorded in D_2O at 298 K (otherwise stated), and DSS (4,4-dimethyl-4-silapentane-1-sulfonic acid) was used as an internal reference. ^1H, ^{13}C, HSQC ($^1H/^{13}C$), and HMBC ($^1H/^{13}C$ and $^1H/^{15}N$) spectra were also recorded at 10, 220, and 120 ppm, for ^1H, ^{13}C, and ^{15}N, respectively. When necessary, a solvent suppression was achieved using an excitation sculpting sequence. pH-titration of HYD was performed at 7.59 and 1.12 mM with NaOD 0.01 M. For LuHYD, the spectra were recorded at 7.55 mM, pD = 7.16 (pD = pH_{read} + 0.41).[38]

Diffusion Coefficient Measurements. The self-diffusion coefficients D^t were measured on a Bruker Nanobay 400 equipped with a BBFO probe 5 mm by applying the bipolar stimulated spin−echo sequence to protons in the complex in D_2O solutions.[39] The proton gyromagnetic ratio is denoted by γ_I, the strength of the gradient pulse by g, the duration of this gradient by δ, and the diffusion delay by Δ. The self-diffusion coefficient D^t was calculated by fitting of the theoretical expression of the proton signal intensity $I(\delta,\Delta,g) = I_0 \exp[-(\gamma_I g\delta)^2(\Delta-\delta/3)D^t]$, in which $I(\delta,\Delta,g)$ and I_0 are the intensities in the presence and absence of the gradient pulses, respectively. The values chosen for δ and Δ in these measurements depend on the magnitude of the diffusion coefficient being measured. For quickly diffusing HOD molecules, the values of δ and Δ were 1 and 100 ms, respectively. For the slowly diffusing complexes, they were 1.5 and 150 ms, respectively. In the experiments, g was increased from 2.2 to 36 G cm^{-1}.

Temperature-Dependent ^{17}O NMR Measurements. The transverse and longitudinal ^{17}O relaxation rates ($1/T_2$, $1/T_1$) and the chemical shifts were measured in aqueous solutions of GdL (14.5 mM, pH = 6.5) in the temperature range 280−350 K, on a Bruker Avance 500 (11.7 T, 67.8 MHz) spectrometer. The temperature was calculated according to previous calibration with ethylene glycol and methanol.[40] An acidified water solution ($HClO_4$, pH 3.3) was used as external reference. Longitudinal relaxation times (T_1) were obtained by the inversion−recovery method, and transverse relaxation times (T_2) were obtained by the Carr−Purcell−Meiboom−Gill spin−echo technique.[41] The technique of the ^{17}O NMR measurements on Gd^{3+} complexes has been described elsewhere.[42] The samples were sealed in glass spheres fitted into 10 mm NMR tubes to avoid susceptibility corrections of the chemical shifts.[43] To improve the sensitivity, ^{17}O-enriched water (10% $H_2{}^{17}O$, CortectNet) was added to the solutions to reach around 1% enrichment. The ^{17}O NMR data have been treated according to the Solomon−Bloembergen−Morgan theory of paramagnetic relaxation (see Supporting Information). The least-squares fit of the ^{17}O NMR data was performed using Visualiseur/Optimiseur[44,45] running on a MATLAB 8.3.0 (R2014a) platform.

Relaxometric Measurements. Proton NMRD profiles ([GdHYD] = 2.99 mM, pH = 6.5) were recorded on a Stelar SMARTracer Fast Field Cycling relaxometer (0.01−10 MHz) and a Bruker WP80 NMR electromagnet adapted to variable field measurements (20−80 MHz) and controlled by a SMARTracer PC-NMR console. The temperature was monitored by a VTC91 temperature control unit and maintained by a gas flow. The temperature was determined by previous calibration with a Pt resistance temperature probe. The longitudinal relaxation rates ($1/T_1$) were determined in water. The least-squares fit of the ^1H NMRD data and simultaneous fit with the ^{17}O NMR data were performed using Visualizeur/Optimiseur[44,45] running on a MATLAB 8.3.0 (R2014a) platform. The influence of the anion was measured for [GdHYD] = 1.28 mM, in Hepes buffer 0.1 M, pH = 7.4 at 298 K, and 20 MHz for citrate and 6 MHz for carbonate and phosphate.

Kinetic Measurements. The rates of the metal exchange reactions of GdHYD were studied by following the formation of the CuHYD complex using conventional UV−vis spectrophotometry (Varian Cary 1E UV−vis spectrophotometer equipped with Varian 1 × 1 Peltier thermostated cell holder) because the decomplexation of GdHYD was sufficiently slow. The exchange reactions were followed at 250 nm in the pH range of 3.34−4.89. The concentration of the complex was 0.1042 mM, while the Cu^{2+} ion was applied at high excess (10−40-fold) to ensure pseudo-first-order conditions. The temperature in the samples was maintained at 25 °C, and the ionic strength of the solutions was kept constant by using 0.15 M NaCl. For keeping the pH constant, dimethylpiperazine (dmp, 50 mM) buffer was used (log K_2^H = 4.19 (0.01) at 25 °C in 0.15 M NaCl). The pseudo-first-order rate constants (k_{obs}) were calculated by fitting the absorbance versus-time data to the following equation:

$$A_t = (A_0 - A_e)\, e^{-k_{obs}t} + A_e$$

DOI: 10.1021/acs.inorgchem.5b00804
Inorg. Chem. 2015, 54, 5991−6003

where A_t, A_0, and A_e are the absorbance at time t, at the start, and at equilibrium, respectively. The fittings were performed with the computer program Micromath Scientist, version 2.0 (Salt Lake City, UT), by using a standard least-squares procedure. The k_{obs} values were reproduced within 2% error as determined in three identical experiments for some of the samples obtained at lower pH.

■ ASSOCIATED CONTENT

Supporting Information

NMR, UV−visible spectra, and potentiometric titration curves. Equations used for the analysis of the ^{17}O data and the NMRD profiles. The Supporting Information is available free of charge on the ACS Publications website at DOI: 10.1021/acs.inorgchem.5b00804.

■ AUTHOR INFORMATION

Corresponding Authors

*E-mail: celia.bonnet@cnrs-orleans.fr.
*E-mail: eva.jakabtoth@cnrs-orleans.fr.

Notes

The authors declare no competing financial interest.

■ ACKNOWLEDGMENTS

We thank Hervé Meudal for his help in recording spectra on the 700 MHz spectrometer. This work was financially supported by the Institut National du Cancer, La Ligue contre le Cancer, and was carried out in the frame of the European COST action TD1004 "Theragnostics Imaging and Therapy: An Action to Develop Novel Nanosized Systems for Imaging-Guided Drug Delivery". G.T. gratefully acknowledges support from the COST Actions CM1006 "European F-Element Network (EuFen)" and also thanks the Hungarian Scientific Research Fund (OTKA K-84291 and K-109029) and the support from the Hungarian-French bilateral Scientific and Technological Cooperation (project no. TÉT_11-2-2012-0010 and PHC Balaton).

■ REFERENCES

(1) Bünzli, J.-C. G. *J. Coord. Chem.* **2014**, *67*, 3706.
(2) Toth, E.; Helm, L.; Merbach, A. In *The Chemistry of Contrast Agents in Medical Magnetic Resonance Imaging*, 2nd ed.; Merbach, A., Helm, L., Toth, E., Eds.; John Wiley & Sons: Chichester, 2013; p 25.
(3) Bonnet, C. S.; Fries, P. H.; Crouzy, S.; Seneque, O.; Cisnetti, F.; Boturyn, D.; Dumy, P.; Delangle, P. *Chem.—Eur. J.* **2009**, *15*, 7083.
(4) Daughtry, K. D.; Martin, L. J.; Sarraju, A.; Imperiali, B.; Allen, K. N. *ChemBioChem* **2012**, *13*, 2567.
(5) Bonnet, C. S.; Fries, P. H.; Gadelle, A.; Gambarelli, S.; Delangle, P. *J. Am. Chem. Soc.* **2008**, *130*, 10401.
(6) Tircso, G.; Garda, Z.; Kalman, F. K.; Baranyai, Z.; Pocsi, I.; Balla, G.; Toth, I. *J. Inorg. Biochem.* **2013**, *127*, 53.
(7) Bonnet, C. S.; Fries, P. H.; Crouzy, S.; Delangle, P. *J. Phys. Chem. B* **2010**, *114*, 8770.
(8) Datta, A.; Raymond, K. N. *Acc. Chem. Res.* **2009**, *42*, 938.
(9) Aime, S.; Calabi, L.; Cavallotti, C.; Gianolio, E.; Giovenzana, G. B.; Losi, P.; Maiocchi, A.; Palmisano, G.; Sisti, M. *Inorg. Chem.* **2004**, *43*, 7588.
(10) Pellegatti, L.; Zhang, J.; Drahos, B.; Villette, S.; Suzenet, F.; Guillaumet, G.; Petoud, S.; Toth, E. *Chem. Commun.* **2008**, 6591.
(11) Bonnet, C. S.; Buron, F.; Caille, F.; Shade, C. M.; Drahos, B.; Pellegatti, L.; Zhang, J.; Villette, S.; Helm, L.; Pichon, C.; Suzenet, F.; Petoud, S.; Toth, E. *Chem.—Eur. J.* **2012**, *18*, 1419.
(12) Caille, F.; Bonnet, C. S.; Buron, F.; Villette, S.; Helm, L.; Petoud, S.; Suzenet, F.; Toth, E. *Inorg. Chem.* **2012**, *51*, 2522.
(13) Bonnet, C. S.; Caillé, F.; Pallier, A.; Morfin, J.-F.; Petoud, S.; Suzenet, F.; Tóth, É. *Chem.—Eur. J.* **2014**, *20*, 10959.
(14) Tei, L.; Benzi, M.; Kielar, F.; Botta, M.; Cavallotti, C.; Giovenzana, G. B.; Aime, S. *Helv. Chim. Acta* **2009**, *92*, 2414.
(15) Baranyai, Z.; Tei, L.; Giovenzana, G. B.; Kálmán, F. K.; Botta, M. *Inorg. Chem.* **2012**, *51*, 2597.
(16) Imperio, D.; Giovenzana, G. B.; Law, G.-l.; Parker, D.; Walton, J. W. *Dalton Trans.* **2010**, *39*, 9897.
(17) Mukkala, V. M.; Sund, C.; Kwiatkowski, M.; Pasanen, P.; Hogberg, M.; Kankare, J.; Takalo, H. *Helv. Chim. Acta* **1992**, *75*, 1621.
(18) Smith, R. M.; Motekaitis, R. J.; Martell, A. E. *NIST Standard Reference Database*; National Institute of Standards and Technology, 1997.
(19) Kapinos, L. E.; Sigel, H. *Inorg. Chim. Acta* **2002**, *337*, 131.
(20) Bates, R. G.; Schwarzenbach, G. *Helv. Chim. Acta* **1954**, *37*, 1069.
(21) Cacheris, W. P.; Nickle, S. K.; Sherry, A. D. *Inorg. Chem.* **1987**, *26*, 958.
(22) Cacheris, W. P.; Quay, S. C.; Rocklage, S. M. *Magn. Reson. Imaging* **1990**, *8*, 467.
(23) Regueiro-Figueroa, M.; Ruscsák, E.; Fra, L.; Tircsó, G.; Tóth, I.; de Blas, A.; Rodríguez-Blas, T.; Platas-Iglesias, C.; Esteban-Gómez, D. *Eur. J. Inorg. Chem.* **2014**, *2014*, 6165.
(24) Rodriguez-Rodriguez, A.; Garda, Z.; Ruscsak, E.; Esteban-Gomez, D.; de Blas, A.; Rodriguez-Blas, T.; Lima, L. M. P.; Beyler, M.; Tripier, R.; Tircso, G.; Platas-Iglesias, C. *Dalton Trans.* **2015**, *44*, 5017.
(25) Baranyai, Z.; Uggeri, F.; Giovenzana, G. B.; Benyei, A.; Brucher, E.; Aime, S. *Chem.—Eur. J.* **2009**, *15*, 1696.
(26) Brücher, E.; Tircso, G.; Baranayai, Z.; Kovacs, Z.; Sherry, A. D. In *The Chemistry of Contrast Agents in Medical Magnetic Resonance Imaging*; Merbach, A. E., Helm, L., Toth, E., Eds.; John Wiley and Sons: Chichester, 2013; p 157.
(27) Sarka, L.; Burai, L.; Brucher, E. *Chem.—Eur. J.* **2000**, *6*, 719.
(28) Tircsó, G.; Kálmán, F. K.; Pál, R.; Bányai, I.; Varga, T. R.; Király, R.; Lázár, I.; Québatte, L.; Merbach, A. E.; Tóth, É.; Brücher, E. *Eur. J. Inorg. Chem.* **2012**, *2012*, 2062.
(29) Beeby, A.; Clarkson, I. M.; Dickins, R. S.; Faulkner, S.; Parker, D.; Royle, L.; de Sousa, A. S.; Williams, J. A. G.; Woods, M. *J. Chem. Soc., Perkin Trans. 2* **1999**, 493.
(30) Fries, P. H.; Belorizky, E. *J. Chem. Phys.* **2005**, *123*, 124510.
(31) Caravan, P.; Ellison, J. J.; McMurry, T. J.; Lauffer, R. B. *Chem. Rev.* **1999**, *99*, 2293.
(32) Halle, B.; Wennerstrom, H. *J. Chem. Phys.* **1981**, *75*, 1928.
(33) Powell, D. H.; NiDhubhghaill, O. M.; Pubanz, D.; Helm, L.; Lebedev, Y. S.; Schlaepfer, W.; Merbach, A. E. *J. Am. Chem. Soc.* **1996**, *118*, 9333.
(34) Botta, M.; Aime, S.; Barge, A.; Bobba, G.; Dickins, R. S.; Parker, D.; Terreno, E. *Chem.—Eur. J.* **2003**, *9*, 2102.
(35) Gale, E. M.; Kenton, N.; Caravan, P. *Chem. Commun.* **2013**, *49*, 8060.
(36) Martell, A. E.; Motekaitis, R. J. *Determination and Use of Stability Constants*; VCH: New York, 1992.
(37) Gans, P.; Sabatini, A.; Vacca, A. *Talanta* **1996**, *43*, 1739.
(38) Glasoe, P. K.; Long, F. A. *J. Phys. Chem.* **1960**, *64*, 188.
(39) Jerschow, A.; Muller, N. *J. Magn. Reson.* **1997**, *125*, 372.
(40) Raiford, D. S.; Fisk, C. L.; Becker, E. D. *Anal. Chem.* **1979**, *51*, 2050.
(41) Meiboom, S.; Gill, D. *Rev. Sci. Instrum.* **1958**, *29*, 688.
(42) Micskei, K.; Helm, L.; Brucher, E.; Merbach, A. E. *Inorg. Chem.* **1993**, *32*, 3844.
(43) Hugi, A. D.; Helm, L.; Merbach, A. E. *Helv. Chim. Acta* **1985**, *68*, 508.
(44) Yerly, F. *VISUALISEUR 2.3.5*; Lausanne, Switzerland, 1999.
(45) Yerly, F. *OPTIMISEUR 2.3.5*; Lausanne, Switzerland, 1999.

DOI: 10.1021/acs.inorgchem.5b00804
Inorg. Chem. 2015, 54, 5991−6003